Damage tolerance of impacted curved panels

L. Ballère, P. Viot, J.-L. Lataillade, L. Guillaumat, S. Cloutet

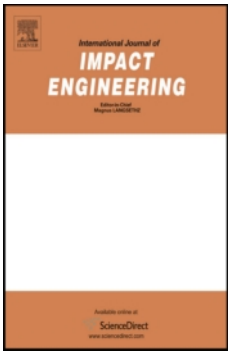

Title: Damage tolerance of impacted curved panels

Authors: L. Ballère, P. Viot, J.-L. Lataillade, L. Guillaumat, S. Cloutet

PII: S0734-743X(08)00070-5
DOI: 10.1016/j.ijimpeng.2008.03.004
Reference: IE 1576

To appear in: *International Journal of Impact Engineering*

Received Date: 17 July 2007
Revised Date: 6 March 2008
Accepted Date: 6 March 2008

Please cite this article as: Ballère L, Viot P, Lataillade J-L, Guillaumat L, Cloutet S. Damage tolerance of impacted curved panels, International Journal of Impact Engineering (2008), doi: 10.1016/j.ijimpeng.2008.03.004

Damage tolerance of impacted curved panels

L. Ballère[1] [a], P. Viot[a], J.-L. Lataillade[a], L. Guillaumat[a] & S. Cloutet[b]

[a]Arts et Métiers - ParisTech, LAMEFIP (Laboratoire Mécanique Endommagement Fiabilité et Ingénierie des Procédés), Esplanade des Arts et Métiers, 33405 Talence Cedex, France

[b]Snecma Propulsion Solide - SAFRAN Group, Les Cinq Chemins, 33187 LE HAILLAN Cedex, France

Abstract

The final aim of this study is to evaluate the influence of impact damage on the residual strength of carbon/epoxy vessels stressed by internal pressure. An intermediate stage determined the residual behaviour of pre-impacted curved panels loaded in tension. Curved panels were impacted, reproducing the damage types observed in impacted vessels filled with propellant. Delamination damage was assessed by ultrasonics and optical microscopy used to observe intra-laminar mechanisms. Tension After Impact (TAI) tests quantified the residual behaviour. An experimental design was used as an alternative to the complex analytical modelling of dynamic damage mechanisms. With this original technique, empirical relationships were established, linking impact parameters to residual properties. The force to failure was found to vary in a bi-linear manner with impact energy. Below a specific level of impact energy corresponding to failure in 4/7 of the plies, there is no significant reduction in the residual strength. The composite Young's modulus decreased linearly with impact energy.

Keywords : residual tensile strength ; composite curved panels ; impact ; experimental design.

1 Introduction

Composite structures can be accidentally damaged by dropping tools, or in collisions with foreign objects in manufacturing, storage or operation. Although it is easy to detect this kind of damage in metallic structures, it is not in composite structures, particularly when the reinforcement used is carbon fibre. Therefore, since it is difficult to avoid accidents, it is necessary to evaluate the effects of damage. There are a number of damage tolerance studies for this kind of material [Cantwell et al., 1986, El-Zein and Reifsnider, 1990, Nettles, 1990, Sjögren et al., 2001, Barkoula et al., 2002, Mitrevski et al., 2006]. The procedure used consists of three steps : i) damage initiation, either using real conditions or reproducing them as closely as possible, ii) damage inspection , evaluating its nature and topology, iii) the quantification of the residual strength, when the structure is stressed under simulated real conditions. Having determined the maximum structural damage that can be tolerated for a given residual strength, there is often a need for structural re-design.

The aim of our study is to evaluate the influence of damage on the residual strength of carbon/epoxy vessels. This generally requires a great number of test results. Study of the real structures is impossible because of the excessive cost involved. Hence specimens are extracted from these structures. In this case, curved panel specimens are extracted from tubes.

Although the literature contains papers concerning the residual burst strength of impacted composite tubes ([Curtis et al., 2000, Gning et al., 2005]), few studies have focused on damage tolerance of composite curved panels, especially when loaded in tension along the longitudinal axis. Our study is a first step to understanding the

physical phenomena which take place when shear or normal stresses (tensile or compressive) are induced at the mesoscale of the multilayered composite. The main damage mechanisms observed, in impacted vessels filled with propellant, are fibre failure and localized delamination. Since fibre failure is the most critical damage mechanism for the tension strength of composite specimens, defect initiation tests were chosen to generate this damage mode and thus cause a significant loss of strength during quasi-static tension tests. Delamination is deliberately limited here to isolate the influence of fibre failure on the residual strength.

Two different methods can be used to predict structural damage due to impact. The first is semi-analytical modelling, in which the interactions between damage mechanisms (fibre failure, delamination ...) and the coupling between local damage and the global response of the structure, are considered. However, the boundary conditions and the contact conditions in impact tests are difficult to evaluate. Since the phenomena occur on a millisecond timescale, it is only possible to identify them experimentally by doing interrupted tests. This strategy was not used because of the small number of samples available.

The second modelling method is empirical using an experimental design [Guillaumat et al., 2004]. This “black-box” model links quantities, representative of damage, to impact parameters. Impact kinetic energy was not chosen as an input, since very different modes of failure can correspond to the same kinetic energy, according to the mass-velocity couple [Guillaumat et al., 2004]. Therefore, we chose to consider the mass and velocity as independent parameters. It is possible to explore a parameter domain, consistent with the real conditions, while minimizing the number of tests required.

2 Material and specimens

The material investigated was made of T800HB carbon fibre and epoxy resin (class 120°C). Known as CS603W, its mechanical properties are listed in Table 1. The fibre volume fraction is 60%. The specimens were cut from tubes manufactured by filament winding.

The tubes were manufactured by winding circumferential layers and longitudinal layers on to a mandrel. With the mandrel rotation axis referred to as the 0° axis, the circumferential layers have 90° orientation and the longitudinal layers have ±20° orientation.

The stacking sequence used for these structures is:

$$Inner-(90°)/[(\pm 20°)/(90°)]_3-Outer$$

which leads to a laminate thickness of 6.54 *mm*. the laminate is not symmetric, and the coupling between in-plane stresses and bending increases the structural vulnerability to global tensile stresses.

The inner radius of the tube, equal to that of the mandrel, is 300 *mm*.

After the unit is processed in a heater to cure the resin, the mandrel and the laminate are separated, and the tube is cut into specimens which are 225 *mm* × 225 *mm* in size (see Figure 1). As a result of cutting, internal stresses from the manufacturing process, are released. This leads to a reduction in the radius of curvature to about 278 *mm*, and some twisting of the panel.

3 Damage initiation

The first step in a damage tolerance study is damage initiation. The experimental device used to simulate potential accidents is as follows.

3.1 Drop tower

An evaluation of potential risks has made it possible to focus the study on low energy impacts such as the dropping of tools. A laboratory drop tower performed these impact tests (Figs. 2 and 3). The specimen is placed in an assembly, clamped to a seismic mass. The drop mass is guided by two vertical columns during the test. A hemispherical indentor, fixed on this mass, has diameter 16 *mm*. A winch raises the drop mass to the desired height, then an electromagnet releases the mass. After the first impact, an anti-bouncing system prevents a second impact.

Sensors are used to measure the impact parameters, and to study the damage phenomena. A piezoelectric force sensor, close to the indentor, measures the contact force between the striker and the specimen. A laser sensor measures the impactor displacement, which includes the indentation depth. Even though the drop height and the falling mass are precisely measured, the impact energy is not equal to the decrease in the drop-mass potential energy, due to friction in the bearings. The impact kinetic energy was obtained from the velocity just prior to impact, which was obtained from the time derivative of the displacement history. Signals from these sensors are taken to a signal conditioner and converted into digital form.

3.2 Specimen mounting device

The main damage mechanism observed during the low-energy impacts is delamination. Fibre failure occurs at higher energies, accompanied by a significant delaminated zone. For composite vessels subjected to an internal pressure, the most critical damage mechanism is fibre failure. Since the specimens are stressed in tension after impact (to reproduce real loading) fibre failure must be favoured, and the delamination zone limited. This also limits the interaction between delamination and free-edge effects [Leguillon et al., 1999]. In order to restrict the damage to a zone close to the impact point, a special device gripped the specimen: Figure 4. The specimen is clamped between two aluminium blocks, tightened with screws. The tightening torque value was chosen by trial and error to achieve good specimen locking and avoid inside face peening.

The specimen is therefore, fully supported on both surfaces except for a circular region of 30 *mm* in diameter in the centre, restricting the delamination damage to within this zone. C.C. Poe, Jr [C.C. Poe et al., 1988] showed that, for composite rings filled with propellant and subjected to impact, the damage is localized to a region directly beneath the impact site. This remark reinforced the choice of the window diameter (30 *mm*) which is close to the impactor diameter (16 *mm*). Although a rectangular shape of this window would have been more in line with the specimen support than this circular shape, the latter was chosen to reproduce the damage shape observed in impacted composite rings filled with propellant. Moreover, the tightening conditions make the influence of the square shape of the support in the impact area negligible.

In order to avoid punching, the sharp-edges of the window are chamfered. The assembly is then placed on the drop tower support. (Figure 3).

3.3 Experimental design

Experimental design is an alternative to analytical modelling based on damage mechanics, which requires the observation and modelling of the interactions between damage mechanisms in impact tests [Lataillade, 2006][Guillaumat et al., 2004]. A response surface is defined by empirical relationships, linking the causes to the consequences. The response surface is determined from discrete experimental points. Interpolation is then used to obtain a continuous function over a defined study field (see Appendix).

In the case of composite curved plates subjected to impact loading, there is no analytical model for the influence of the target properties (stacking sequence, dimensions and curvature) and the impact parameters (impactor mass and velocity, boundary conditions, contact nature) on the structural responses (contact force, deflection, damage, residual behaviour ...). The idea of this study is to calculate a response surface between impact parameters and corresponding residual behaviour.

In order to reduce the experimental cost and to simplify this preliminary investigation only the influences of the impactor mass and the drop height were considered. The drop mass will be represented by the variable x_1 and the drop height by the variable x_2. However, for experimental reasons the x_1 value for experiment *n*°4 (Appendix Table 8). was changed from 0.5 to 1. The effect on the model accuracy will be quantified by the variance study presented at the end of this paper.

In order to determine the physical values corresponding to each experiment of the selected design, it is necessary to choose the boundary values for each variable. These values are associated with the maximal non-dimensional data of Doelhert's matrix [Doelhert, 1970, Doelhert and Klee, 1972] (see Appendix). Therefore, x_1 equals -1 for the minimum impactor mass and +1 for the maximum mass. Likewise, x_2 equals -1 for the minimum drop height and +1 for the maximum height. A conversion is then made between the physical and non-dimensional variables. The physical values for the experiments are listed in Table 2.

3.4 Results of impact tests

For each point of the experimental design, three specimens were tested. To establish a relation between the impact parameters and the consequent strength degradation, it is necessary to estimate the damage precisely. To do this, microscopy (a destructive test) was used for each of the two fibre orientations (20° and 90°) and a third non-destructive test used ultrasonic mapping of the delaminated zone (this specimen is later used for a quasi-static test of residual tensile strength).

3.4.1 Repeatability of the impact test specimen response.

Three repeat impact tests were used to establish the relation between the damage and the residual tensile strength. There is good repeatability of the specimen response in the impact tests. Figures 5 and 6 respectively show the response of three specimens for impact experiment *n*°3 (the lowest energy level) and experiment *n*°4 (the highest energy level). Each figure shows the contact force variation with the impactor displacement. These two energy levels, at the bounds of the experimental design, were analyzed to find the influence of the damage on the repeatability of the specimen response.

The energy level represented in Figure 5 corresponds to a damage which cannot be detected by visual inspection. The maximum variation in kinetic energy, of about 4.2%, is caused by a variation in the impact velocity due to variable friction in the bearings on the guidance columns (fig. 3)(the maximum variation in velocity is 2.1%). With such a low variation in the impact velocity, the response of the specimens is similar. The shape is approximately the same, with three stages: i) an initial force peak when the impactor contacts the specimen, ii) a force increase to a maximum, iii) specimen unloading. The variation in the maximum force is 1.9% and in the maximum displacement 4.3%. This demonstrates the repeatability of the specimen responses when there is moderate damage.

Figure 6 shows the specimen response during impact tests performed with an energy of about 70 *J*, in which the specimen is severely damaged. As previously found the variation in the impact velocity is small ; it is 0.04 $m.s^{-1}$, or 1.2% and the variation in kinetic energy is 2.4%. As previously found, the response is similar for the three specimens. For each test, the shape of the force/displacement curve consists of the first two stages described previously, then, iii) pronounced damage where the force keeps a quasi-constant, plateau value and finally, the specimen unloading. The variation of the maximum force is 16.4% and that of the maximum displacement is 3%. Although the observed force variation is rather significant, two of the three specimens exhibit a variation equal to 6%. Since the fracture of composite materials is generally dispersed, the repeatability of the specimen response in the case of a pronounced damage can be considered acceptable.

3.4.2 Experimental design realization

Since the specimen behaviour has a low uncertainty, it is possible to conduct the previously-described test campaign associated with the experimental design. Figure 7 illustrates the contact force variation with impactor displacement. Since repeatability was demonstrated in the previous subsection, for clarity only one test for each point of the experimental design is presented in this figure.

As mentioned before, for each mass/velocity couple, a first force peak is observed and it keeps a quasi-constant value. The maximum contact force then increases with the impact energy in a non-linear way. From low energy levels (22 *J* at Point A), an impact energy increase by 29% to Point B causes a strong increase in the contact force (29%). It is difficult to be sure that this increase is only due to the kinetic energy increase. It would be wiser to consider the influence of the mass and the velocity separately. However, from a higher energy level of 54 *J*, at Point C, an increase of 22% of the kinetic energy (Point D) only causes a 4.5% increase in the maximum force. This non-linearity of response is illustrated in Figure 8. Although higher energy levels were not investigated, the maximum force seems to tend to an asymptotic value of about 25000 *N*. This level corresponds to the maximum force that can be sustained by the structure in this test configuration.

4 Damage assessment

The damage assessment was the second step of the study. The suspected damage mechanisms were delamination and fibre failure. To detect these, ultrasonic non-destructive inspection was used for delamination and optical microscopy examination for fibre failure.

4.1 Non-destructive inspection (ultrasonics)

The aim of this non-destructive inspection is not to present very detailed C-scan graphs but only to affirm that the delaminated zone is included in a cylinder of 30 *mm* in diameter, corresponding to the impact area.

The specimen was set on a C-channel with the concave face upwards completely immersed in water, in an ultrasonic tank. The diameter of the ultrasonic transducer was 6 mm. It was non-focused and its frequency was 10 MHz. The transducer axis is normal to the axis of the cylindrical specimen (normal incidence) and the specimen was scanned parallel to the cylinder axis. The resulting signal, observed on an oscilloscope screen, detects the beginning and the end of delamination. The specimen is then rotated about the cylinder axis and scanned again parallel to that axis. The step between two scans is 10 mm.

Figure 9 illustrates the typical result obtained by this technique. The specimen dimensions (225 mm x 225 mm) are shown and the triangle at the centre corresponds to the impact point. The scan lines are vertical. Along each scan line, the two points shown correspond to the upper and lower boundaries of the delaminated zone (distance D_1). The horizontal error bar is the diameter of the transducer i.e. 6 mm. Since the delamination is detected when the signal changes significantly, the vertical error is estimated at 2 mm. We assumed that the delamination zone has a circular shape (i.e $D_2 = D_1$). This assumption is verified by optical microscopy presented in the following sub-section. The error on the diameter is estimated at 2 mm.

For the different impact tests, the delaminated zone was included in a cylinder of 30 ± 2 *mm* in diameter.

4.2 Optical microscopy

The specimens were cut for optical microscopy examination, to detect damage mechanisms such as fibre failure and, matrix cracking.

The specimens are cut with a diamond circular saw, with a high rotation velocity and a very low feed velocity, to limit damage. To observe the failure of the circumferential fibres, the sample was sectioned circumferentially, as shown on the left side of Figure 10 a). To observe longitudinal fibres, the sectioning was done along the 20° fibre angle, as shown on the right side of Figure 10 a).

The sectioned samples were coated with an epoxy resin and the surface polished with a 1 μm grade abrasive.

The appearance of polished samples (Figure 10 b), changes according to the cutting orientation. When cut parallel to circumferential fibres (oriented at 90°), these fibres look more or less like continuous lines, while the longitudinal fibres have elliptical cross-sections.

When cut parallel to the longitudinal fibres (for example +20°), these appear as continuous lines while those oriented at -20°, have elliptical cross-sections. Circumferential fibres appear with a more or less circular cross-section.

Therefore, depending on the cutting direction, one can either observe the failure of fibres oriented at +20°, or those oriented at -20°. It is not possible to confirm that a longitudinal layer has completely failed by fibre fracture.

With the specimen mounting device used in this study, many damage mechanisms appear as shown in Figure 11. One can observe delamination, matrix cracking, and fibre failures. Particular attention was paid to fibre fracture since this is the most critical damage mechanism for the tension strength. Three types of fibre failures can be observed: i) those due to local shear stresses (type n^o1 Figure 11), ii) self-organized failures linked to bending stresses (i.e. kink-bands [Zhou, 1996]) and, iii) failures without any organization (type n^o2 Figure 11).

Cutting along the circumferential fibres made it possible to verify the assumption of a circular shape delamination zone, as shown in Figure 12. Measuring the size of the larger delamination (highlighted in this figure) which corresponds to the projected zone measured by ultrasonics, it is possible to affirm that the distance D_2 is equal to $D_1 \pm 2$ *mm* (Figure 9) for each impact energy level. Hence the delamination zone is always included in a cylinder of 30 ± 2 *mm* in diameter.

The results of the microscopic observations of fibre failures are presented in Table 3. Although increased energy level is not the only factor responsible for increased damage (it should be more rational to consider the mass/velocity couple), the columns of this table are ranked in order of increasing theoretical (i.e. potential) impact energy. Each row is associated with a specific layer of the laminate. The coloured cells represent layers in which fibre fractures were observed. “NFD” means that no failure was detected in the examined zone. The empty cells correspond to the previously reported indeterminate results, where fibre fractures could not be confirmed.

Considering the whole table, there is an increase in the number of failed layers with increasing impact energy. Although the extent of the damage is not mentioned in the

table, it increases with depth. A conical shape was observed with its vertex located close to the impact point. This pine-tree shape is usually observed in the case of thick laminates [Abrate, 1998].

5 Residual tensile strength

The determination of the residual tensile strength of impacted specimens is the last phase of the study.

5.1 Specimen preparation

Since the projected area of the delaminated zone was determined by ultrasonics, the 225 *mm* × 225 *mm* specimens were cut, with a diamond saw, on both sides of the damage zone to obtain a 225 *mm*× 70 *mm* specimen (see Figure 13). Undamaged specimens were also cut to the same dimensions. Reinforcement tabs were cut from of similar material with the same thickness and curvature. Their dimensions are 70 × 50 *mm* and they are chamfered on one of the 70 *mm* lengths at a 45° angle to minimize the effect of shear stresses. The tabs were bonded to the specimen with an epoxy resin. The assembly is then pressed for 24 hours for the adhesive to cure. The interface between the jaws of the tensile machine and the curved assembly is made of aluminium parts, which ensure uniform tightening on the tabs during the tensile test. In order to avoid slipping between the aluminium parts and the carbon/epoxy tabs, they are also bonded with the same epoxy resin and subjected to uniform pressure for 24 hours for the glue to cure. The assembly, aligned with the jaws of the tensile machine, is detailed in Figure 13.

In order to quantify the conventional longitudinal strain along the tensile machine axis, a laser extensometer continually measured the distance between two reflecting targets stuck on the specimen.

Curves representing the variation of the conventional longitudinal stress with the associated strain were linearly interpolated to calculate the slope and hence the mean homogenized elastic modulus.

5.2 Results of quasi-static tests

5.2.1 Undamaged specimens

Since the aim of this study is to quantify the residual tensile strength variation of damaged specimens compared to undamaged ones, a first series of runs was conducted on non damaged specimens. A typical stress-strain curve is shown in Figure 14 together with the straight-line fit used to calculate the mean homogenized elastic modulus. The behaviour of undamaged specimens can be considered quasi-linear. Nevertheless, one can observe slope variations of the stress *vs* strain curve. During the tensile tests, due to the lay-up and the boundary conditions, the specimen curvature tends to increase between the jaws. Therefore, for a strain value close to 1000 *μdef*, circumferential layers (i.e. 90^o oriented) are progressively damaged according to the interfibre mode causing the elastic modulus to decrease. This progressive damage changes the orientation of fibres oriented at $\pm 20^o$ towards the loading direction (0^o) and the homogenized elastic modulus increases (for a strain value close to 1500 *μdef*). The specimen exhibits a linear behaviour until the final failure. The stress plateau at this end of the strain-stress curve corresponds to the failure of the layer to which the laser extensometer reflecting targets

are stuck. When failure occurs, the distance between these two targets increases considerably, and leads to a strong increase of the strain.

Table 4 presents the results from these tests. The mean force to failure is 160.9 *kN* and the variation coefficient, calculated from the ratio $\frac{standard\ deviation}{mean}$, is equal to 5.7%. The result is acceptable if we consider the dispersion generally observed in the failure of composite laminates.

The mean homogenized elastic modulus has a mean value of 50.6 *GPa* and a variation coefficient equal to 4.9%. This elastic modulus value is analytically derivable with the classical laminate theory. The elastic modulus obtained by calculation is 58.8 *GPa.* The variation with respect to the experimental value is 14%. The observed deviation could be explained by the fact that the classical laminate theory is based on the thin plate assumptions where the transverse shear stresses are neglected. In this case, the ratio $\frac{thickness}{width}$ is such that this theory is not applicable.

5.2.2 Pre-damaged specimens

The influence of different amounts of impact damage on the residual tensile behaviour of the specimens is illustrated in Figure 15. The reference curve is for an undamaged specimen. There is a global decrease of the mean homogenized elastic modulus according to the initial damage state of the specimens. The previously-described phenomenon, which explain the variation in slope of the stress-strain curves at the beginning of the test, occurs for each test of pre-damaged specimens. Other variations in elastic modulus occur during the tests of damaged specimens. These are

amplified by the initial damage state. It can be assumed that the damage initiated by impact generates a local anisotropy which leads to a modification of the specimen behaviour during tensile tests.

The impact damage influences the residual tensile strength of the specimens. Figure 16 shows the variation of the maximum force to failure with the impact energy. Point A, for undamaged specimens occurs at the mean force presented in Table 4. For impact energies lower than 40 *J*, the damage seems to have no significant influence on the residual tensile strength. This energy level corresponds to failure, in a cylinder of 30 mm in diameter at the specimen center, of 4 of the 7 plies (50% of these plies are oriented at 90°). From this energy level, the maximum force to failure starts to decrease until the maximum impact energy level at which all the plies are failed. At this point, the loss of strength with respect to the undamaged specimens is 18.6 %. One can note that, while Table 3 shows the similar degree of fibre fracture for impact energies of 40 *J* and 53 *J*, there is no reduction of the residual tensile strength for the first energy level. We assume that the force to failure depends, both on the number of failed layers and the location, through the thickness, of the fibre failures.

While the failure force versus impact energy graph consists of two linear regions, the homogenized elastic modulus seems to decrease linearly with impact energy (Figure 17). The elastic modulus of undamaged specimens is presented in Table 4. The maximum loss of elastic modulus, for the highest energy level of 69 *J*, is 46 %. Considering that the longitudinal elastic modulus is mainly determined by the longitudinal fibres, this reduction seems acceptable when most of the fibres have failed.

The residual force to failure as a function of the impact mass and the drop height is shown by the response surface in Figure 18. This plot, directly established from the experimental design analysis, indicates the influence of each input parameter on the force to failure. Therefore, one can note that there is not a preponderant parameter on the residual tensile strength.

The second degree polynomial used for the interpolation of this response is as follows :

$$y = b_0 + b_1 x_1 + b_2 x_2 + b_{11} x_1^2 + b_{22} x_2^2 + b_{12} x_1 x_2 \quad (1)$$

Polynomial factors b_i , b_{ij} are presented in Table 5. The coupling between the mass and the height, associated with b_{12}, is quite small since its value (-2406) is small in comparison with the other factors.

In order to quantify the accuracy of the polynomial model at Point A, it is possible to plot the associated variance function (d_A) as shown in Figure 19. This is calculated by:

$$Var(\hat{y}_A) = x'_A (X'X)^{-1} x_A \sigma^2 \quad (2)$$

where $\hat{y}_A$ is the value of the calculated response at Point A, x_A is associated with the coordinates of Point A.

The high values of this function at the boundaries of the investigated domain correspond to places where the model accuracy is less consistent. The maximum value

is located at the point corresponding to experiment n^o4, which was modified with respect to Doelhert's matrix.

Another way to quantify the accuracy of the model is to analyze the variance (Table 6). The column "Signif" indicates if the measured variation is physical or due to the experimental scattering. The value observed for this parameter is very high (i.e. 36.4). Nevertheless, since the variation of the residual strength is quite small and close to the experimental deviation, this parameter cannot be strictly representative of the model accuracy.

In order to validate this model, the deviation between the experimental measurements and the model (regression) prediction at the points used to define this response surface is presented in Table 7. The maximal deviation of 2.6 % is acceptable.

6 Conclusions

For this study, a specific procedure has been set up to quantify the residual tensile strength of impacted composite vessels filled with propellant. In order to reduce the cost of the experimental tests, the specimens used were curved plates extracted from tubes. An experimental design was used to link impact parameters to the residual tensile strength of specimens. This methodology reduces the number of specimens required.

Impact tests reproduced specific types of accidental damage such as from falling tools. Previous quasi-static tensile tests showed that delamination can interact with the free edges effects in the case of samples. Since a tube has no free edges, a device has been designed to restrict the delamination zone to the specimen center and limit this

interaction. The influence of fibre failure on the residual tensile strength could then be quantified, for a constant delamination area.

The damage was assessed with different techniques. The impact damage using the mounting device designed for this study is close to a damage type observed in vessels filled with propellant and subjected to impact.

In order to quantify the residual tensile strength, quasi-static tests were carried out. These tests showed a bi-linear variation of the maximum force to failure with impact energy. Below a specific level of energy, corresponding to failure in 4⁄7 of the plies, there was no significant reduction in the residual strength. Above this yield energy level, the strength decreases drastically and fracture instabilities occur.

The experimental design used to establish empirical polynomials representing this output parameter (residual tensile strength) has shown that there is no influence of the mass/height couple (impact conditions) on the residual tensile strength in the range used for each input parameter.

Since the residual tensile strength decreases when the specimens are loaded in the longitudinal direction, the next step of this study will be to establish a numerical model which predicts the failure of structures.

References

[Abrate, 1998] Abrate, S. (1998). *Impact on composite structures*. Cambrige University Press.

[Barkoula et al., 2002] Barkoula, N.-M., Papanicolaou, G., and Karger-Kocsis, J. (2002). Prediction of the residual tensile strengths of carbon-fiber/epoxy laminates with and without interleaves after solid particle erosion. *Composites Science and Technology*, 62:121–130.

[Box et al., 1987] Box, G., Hunter, J., and Hunter, W. (1987). *Statistics for Experimenters: An Introduction to Design, Data Analysis, and Model Building*. Wiley and Sons.

[Cantwell et al., 1986] Cantwell, W., Curtis, P., and Morton, J. (1986). An assessment of the impact performance of CFRP with high strain carbon fibres. *Composites Sci and Technol*, 25:133–148.

[C.C. Poe et al., 1988] C.C. Poe, J., Harris, C., and Morris, D. (1988). Surface crack analysis applied to impact damage in a thick graphite/epoxy composite. Technical Report TM-100600, NASA.

[Curtis et al., 2000] Curtis, J., Hinton, M., Li, S., Reid, S., and Soden, P. (2000). Damage, deformation and residual burst strength of filament-wound composite tubes subjected to impact or quasi-static indentation. *Composites : Part B*, 31:419–433.

[Doelhert, 1970] Doelhert, D. (1970). Uniform shell designs. *Applied Statistics*, 19(3):231–239.

[Doelhert and Klee, 1972] Doelhert, D. and Klee, V. (1972). Experimental designs through level reduction of the d-dimensional cuboctahedron. *Discrete Mathematics*, 2:309–334.

[El-Zein and Reifsnider, 1990] El-Zein, M. and Reifsnider, K. (1990). On the prediction of tensile strength after impact of composite laminates. *J. Composites Technology and Research*, 12(3):147–154.

[Gning et al., 2005] Gning, P., Tarfaoui, M., F.Collombet, Riou, L., and Davies, P. (2005). Damage development in thick composite tubes under impact loading and influence on implosion pressure: experimental observations. *Composites : Part B*, 36:306–318.

[Guillaumat et al., 2004] Guillaumat, L., Baudou, F., de Azevedo, A.-M. G., and Lataillade, J.-L. (2004). Contribution of the experimental designs for a probabilistic dimensioning of impacted composites. *International Journal of Impact Engineering*, 31:629–641.

[Lataillade, 2006] Lataillade, J.-L. (2006). Dynamic tests. In FRANCOIS, D., editor, *Structural components*, Mechanical tests and behaviour laws, chapter 9. A. HERMES SCIENCE and LAVOISIER Company Publishers. ISBN 1905209185.

[Leguillon et al., 1999] Leguillon, D., Marion, G., Harry, R., and Lecuyer, F. (1999). The onset of delamination at stress-free edges in angle-ply laminates - analysis of two criteria. *Composites Science and Technology*, (61):377–382.

[Mitrevski et al., 2006] Mitrevski, T., Marshall, I., and Thomson, R. (2006). The influence of impactor shape on the damage to composite laminates. *Composite structures*, 76:116–122.

[Nettles, 1990] Nettles, A. (1990). Instumented impact and residual tensile strength testing of eight-ply carbon/epoxy specimens. Technical Report 2981, NASA.

[Sjögren et al., 2001] Sjögren, A., Krasnikovs, A., and Varna, J. (2001). Experimental determination of elastic properties of impact damage in carbon fibre/epoxy laminates. *Composites : Part A*, 32:1237–1242.

[Zhou, 1996] Zhou, G. (1996). Effect of impact damage on residual compressive strength of glass-fibre reinforced polyester (GFRP) laminates. *Composite Structures*, 35:171–181.

Appendix : Experimental design methodology

Many different models can be chosen for an experimental response prediction (linear or non-linear models, differential equations ...). In the case of a continuous response, the simplest model is a Taylor series. The choice of the degree of polynomial employed is a compromise between the model accuracy and the number of tests to be performed for determination of the polynomial coefficients.

In this study, we postulate a second degree polynomial P function of the impactor mass M and the drop height H, that models the structural responses:

$$P(M,H) = I + aM + bH + cM^2 + dH^2 + eMH \qquad (3)$$

where I,a,b,c,d,e are the coefficients assigned to the input data. The last term eMH corresponds to the coupling between the mass and the height.

The main advantage of a second degree polynomial, compared with a first order polynomial, is its ability to consider non-linear responses, and to couple the different variables.

In order to facilitate the determination of the influence of the respective parameters, the variable coordinates are centered and reduced. Their variation magnitude is bordered in the [-1 , +1] interval applying the transformation :

$$x_j = \frac{u_j - u_j^0}{\Delta u_j} \tag{4}$$

where x_j is the value of the coded variable j (in centred and reduced coordinates), u_j the value of the corresponding natural variable, u_j^0 the value of the natural variable j at the field center.

Δu_j, called the variation step, is defined as follows :

$$\Delta u_j = \frac{u_j^{\max} - u_j^{\min}}{2} \tag{5}$$

Each response, experimentally measured, will be interpolated with the polynomial model y, expressed in centered reduced coordinates, such as :

$$y = b_0 + b_1 x_1 + b_2 x_2 + b_{11} x_1^2 + b_{22} x_2^2 + b_{12} x_1 x_2 \tag{6}$$

The objective is then to identify these parameters b_{ij}. Equation 6 can be written as :

$$Y = XB + e \tag{7}$$

where Y represents the experimental response vector, X the model matrix, B the column vector of the input parameters and e the column vector of the experimental errors.

In order to determine this vector B, the least-square method is used. If the matrix $X'X$ is non singular, then :

$$B = \left(X'X\right)^{-1} X'Y \tag{8}$$

The accuracy of the estimators B is calculated from the variance-covariance matrix defined as follows:

$$Var\left(B\right) = \sigma^2\left(X'X\right)^{-1} \tag{9}$$

where σ is the uncertainty in the experimental measurements. This variance-covariance matrix is independent of experimental results ; it can be determined before the tests because it only depends on the measurement error variance and on the elements of the experimental matrix X.

To identify the polynomial factors, there are many optimal experimental distributions according to the most common polynomial models. [Box et al., 1987].

For this study, a Doelhert experimental matrix was chosen [Doelhert, 1970][Doelhert and Klee, 1972] which makes it possible to use a second degree polynomial (Eq. 6). Its representation in an experimental field with two variables is illustrated in Figure 20.

The experimental point distribution is regular in the selected field. This makes it possible to cover the whole field, without proposing, a-priori, any representative response model. Doelhert's matrix [Doelhert, 1970], in the case of two experimental variables, is shown in Table 8.

Nomenclature

E_i	tensile modulus of the unidirectional ply
G_{ij}	shear modulus of the unidirectional ply
E_{xx}	homogenized elastic modulus of the laminate
H	drop height
V	impact velocity
g	acceleration of gravity
T	kinetic energy
D_i	diameter of the delaminated zone
x_j	value of the coded variable j in centered and reduced
b_{ij}	polynomial factors
X	model matrix
u_j	value of the natural variable j
u_j^0	value of the natural variable j at the field center
Δu_j	variation step
B	column vector of imput parameters
e	column vector of the experimental errors
Greek letters	
v_{ij}	Poisson's ratio of the unidirectional ply
σ_{ij}^R	Ultimate tensile strength of the unidirectional ply
σ_{xx}	conventional stress
ε_{xx}	conventional strain
σ^2	experimental variance

$E_{11}(GPa)$	$E_{22}(GPa)$	$G_{12}(GPa)$	ν_{12}	ν_{21}	$\sigma_{11}^{R}(MPa)$	$\sigma_{22}^{R}(MPa)$
165	7.1	3.9	0.39	0.015	2610	38

Table 1 : Mechanical properties

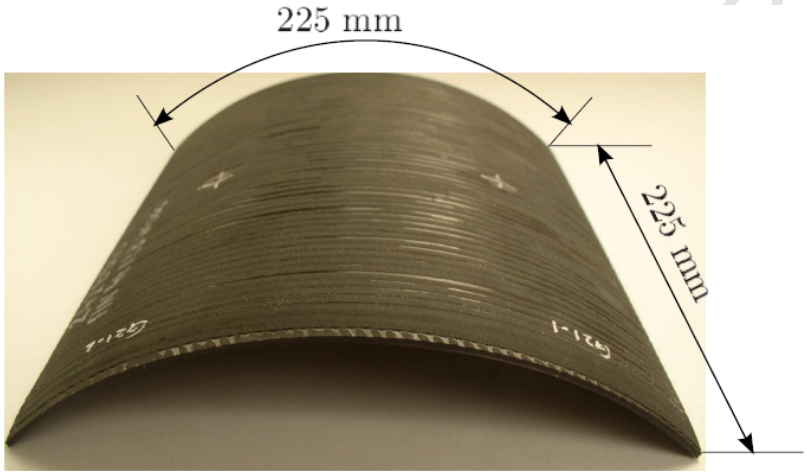

Figure 1 : Specimen

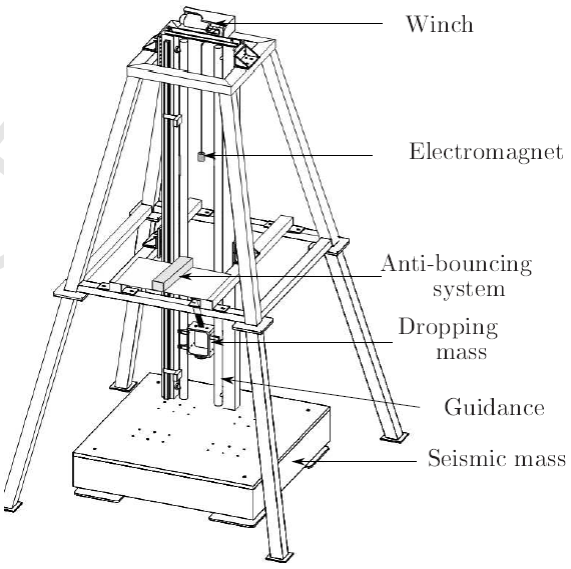

Figure 2 : Global drop tower

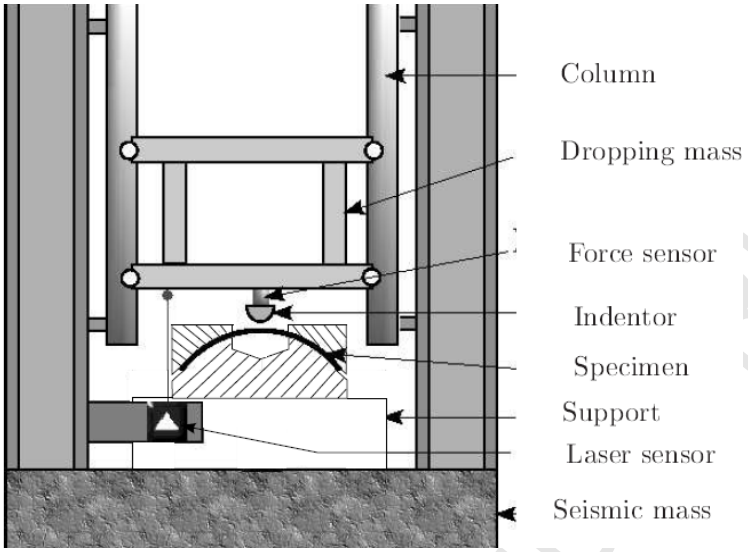

Figure 3 : Detailed drop tower

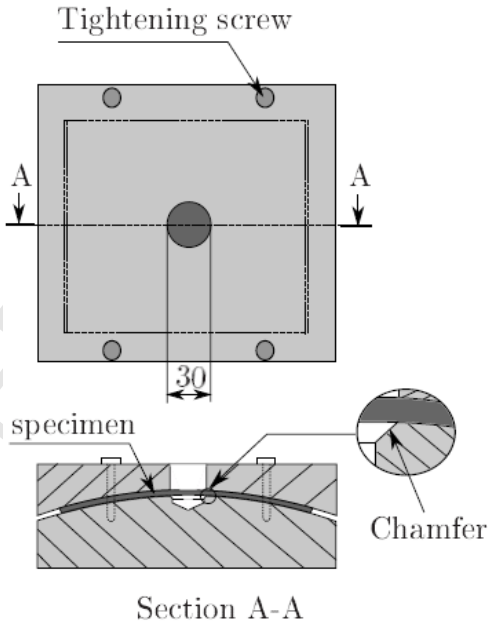

Figure 4 : Specimen mounting device

Experiment	Mass (kg)	Height (m)	Potential energy (J)
1	10,22	0,375	37,60
2	14,48	0,375	53,27
3	5,96	0,375	21,93
4	14,48	0,5	71,02
5	8,09	0,25	19,84
6	12,35	0,25	30,29
7	8,09	0,5	39,68

Table 2 : Experimental design for impact tests

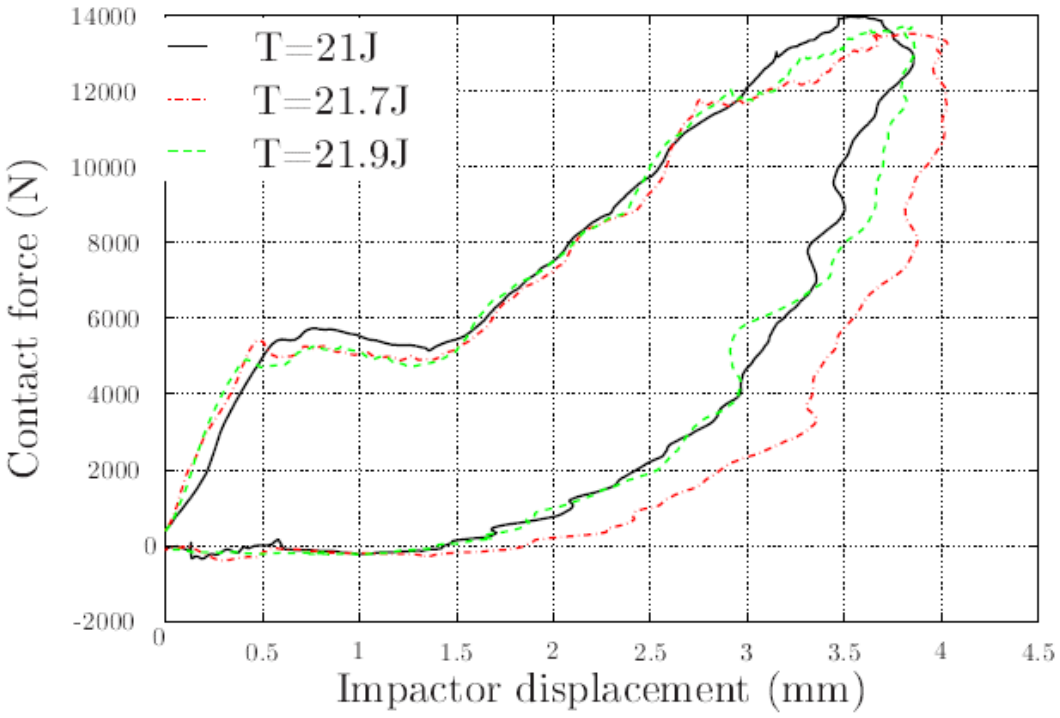

Figure 5 : Repeatability of the specimen responses in the case of a moderate damage

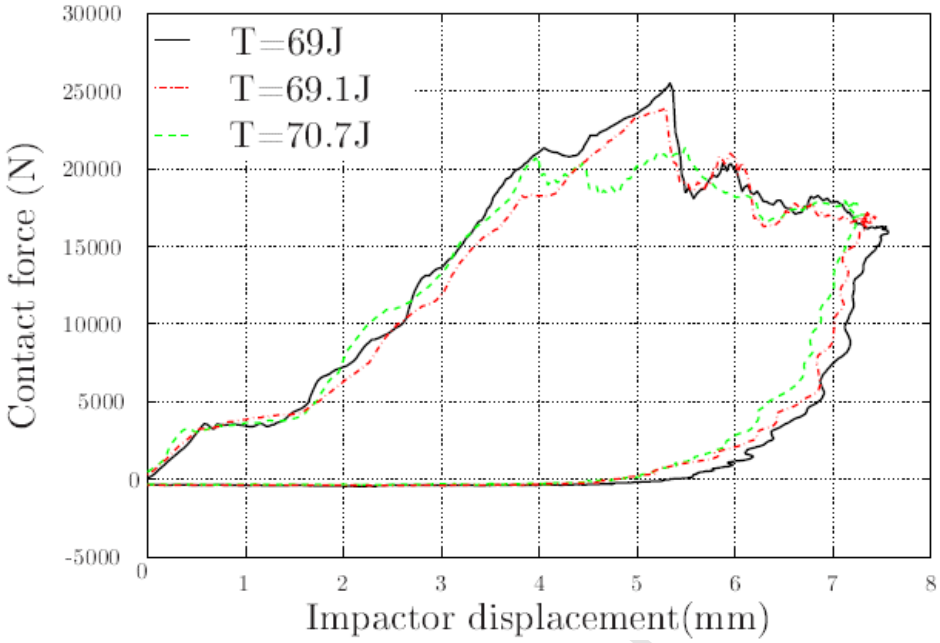

Figure 6 : Repeatability of the specimen responses in the case of a pronounced damage

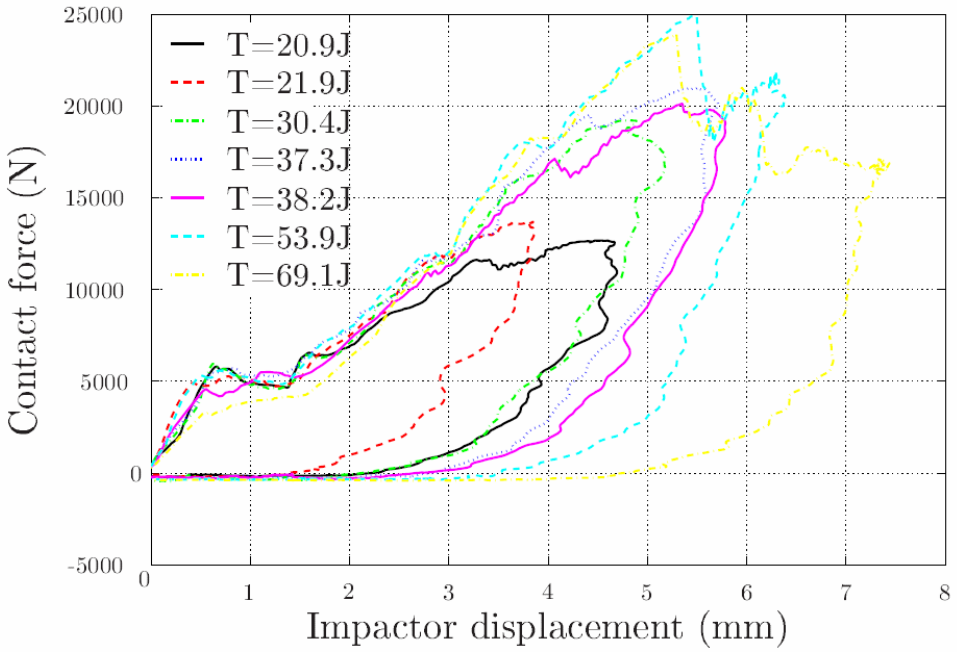

Figure 7 : Force / displacement curves of specimens stressed by impact

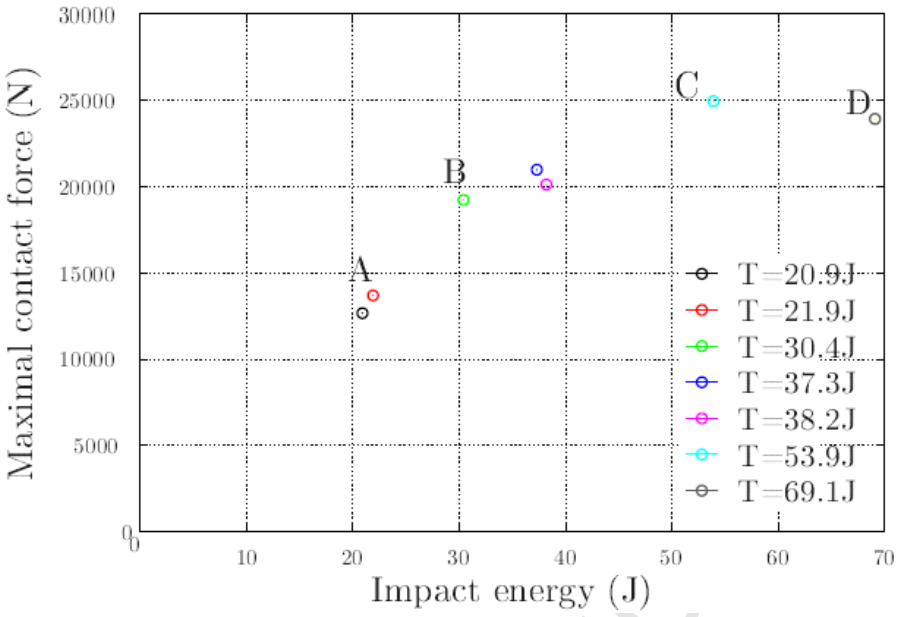

Figure 8 : Maximal contact force evolution according to impact energy

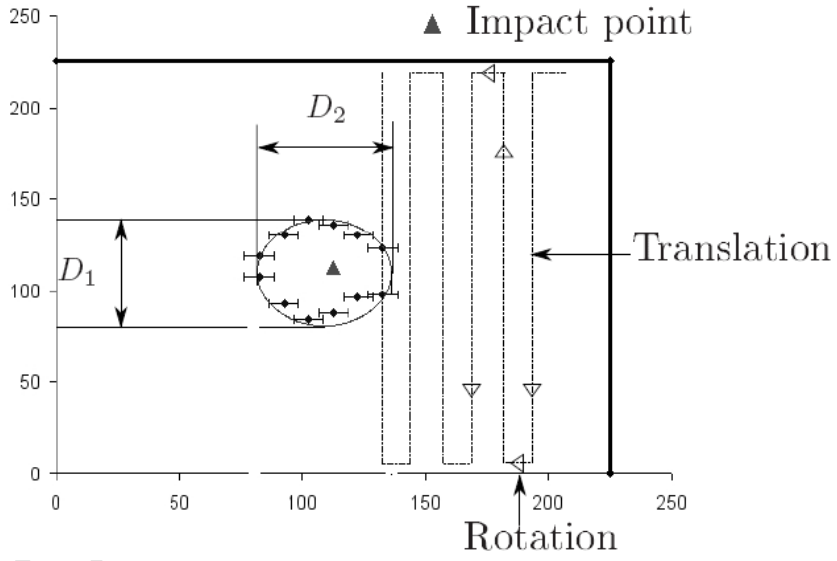

Figure 9 : Ultrasonic inspection result

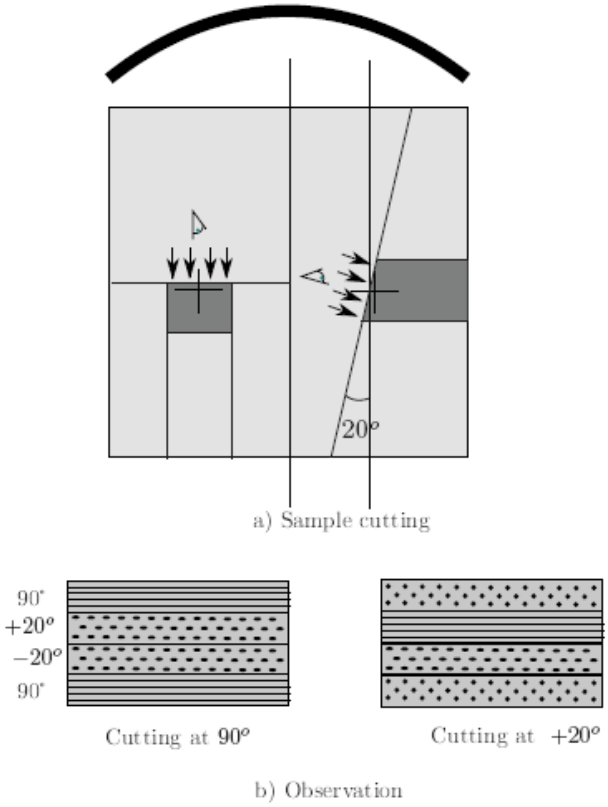

Figure 10 : Procedure for microscopic observation

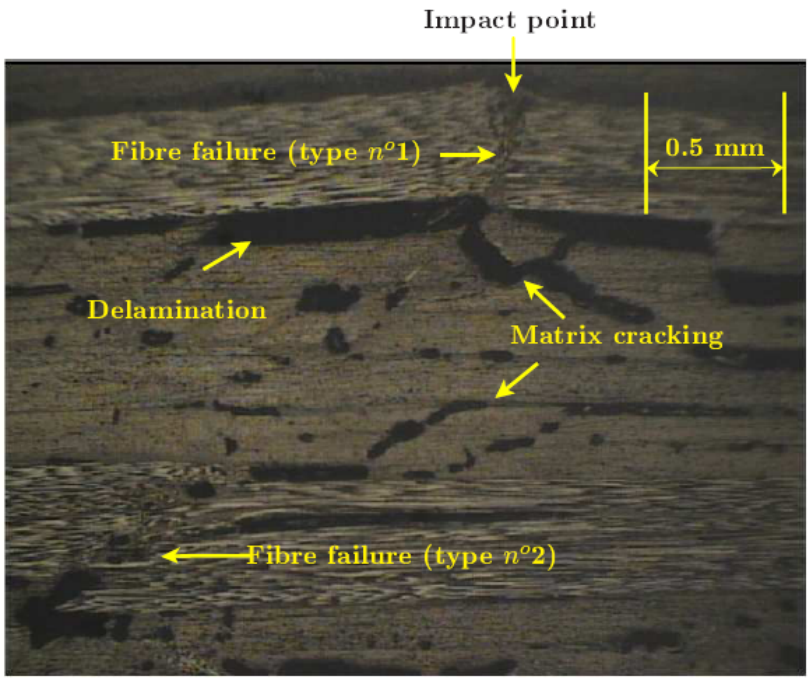

Figure 11 : Microscopic observation presenting the damage mechanisms observed

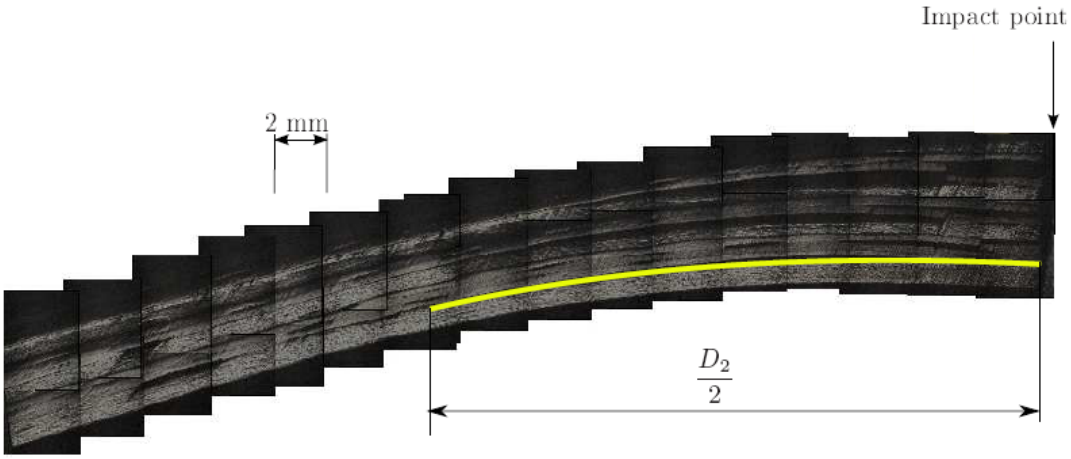

Figure 12 : Microscopic observation presenting the delamination observed

Mass (kg)	8,09	5,96	12,35	10,22	8,09	14,48	14,48
Theoretical velocity (i.e $V = \sqrt{2gH}$) ($m.s^{-1}$)	2,21	2,71	2,21	2,71	3,13	2,71	3,13
Theoretical energy (J)	19,76	21,89	30,16	37,53	39,63	53,17	70,93
Specimen	K22-2	K20-2	K21-2	K19-2	K16-2	K18-2	K17-2
Circumferential 1 (Outer)	fibre failure	fibre failure	fibre failure	fibre failure	fibre failure	fibre failure	fibre failure
Longitudinal 1 ($+\alpha$)		fibre failure	fibre failure			fibre failure	
Longitudinal 1 ($-\alpha$)	fibre failure			fibre failure	fibre failure		fibre failure
Circumferential 2	NFD	NFD	fibre failure	NFD	fibre failure	fibre failure	fibre failure
Longitudinal 2 ($+\alpha$)		NFD	NFD			fibre failure	
Longitudinal 2 ($-\alpha$)	NFD			fibre failure	fibre failure		fibre failure
Circumferential 3	NFD	NFD	NFD	NFD	NFD	NFD	fibre failure
Longitudinal 3 ($+\alpha$)		NFD	NFD			fibre failure NFD	
Longitudinal 3 ($-\alpha$)	NFD			NFD	NFD fibre failure		fibre Failure
Circumferential 4 (Inner)	NFD	NFD	NFD	fibre failure	NFD	NFD	fibre failure

NFD = No Failure Detected

Table 3 : Microscopic observations of impacted specimens

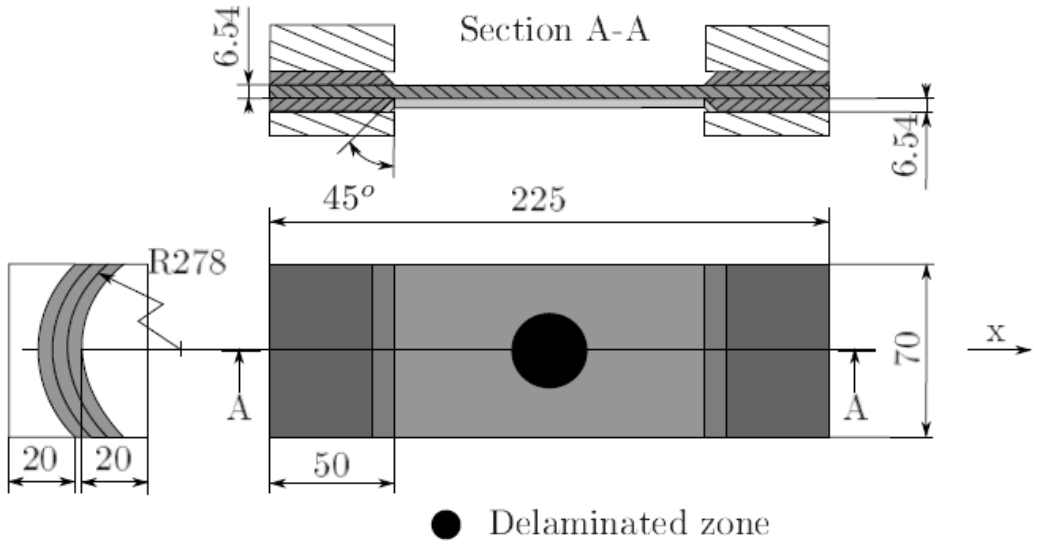

Figure 13 : Geometry of the tensile specimens

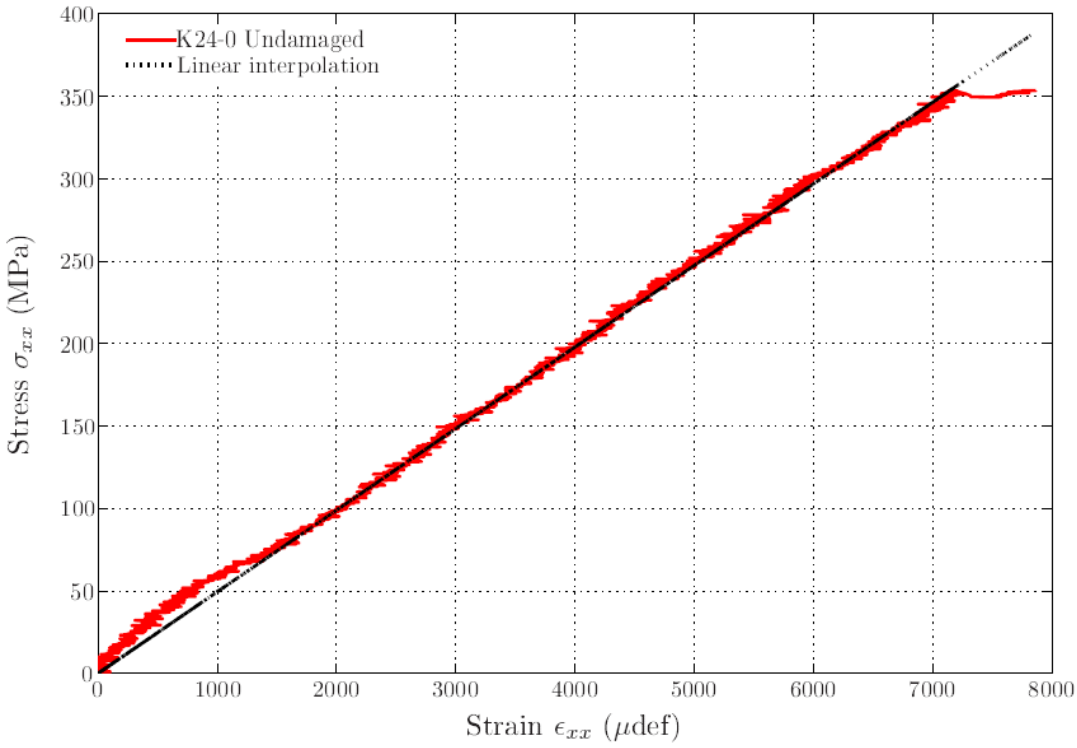

Figure 14 : Typical stress-strain curve in the case of undamaged specimens

Specimen	K3	K13	K15	K23	K24
Force to failure (kN)	152.8	175	162.5	152.5	161.8
Mean force to failure (kN)	160.9				
Variation coefficient (%)	5.7				
elastic modulus (GPa)	52.5	52.5	46.7	51.5	49.5
Mean elastic modulus (GPa)	50.6				
Variation coefficient (%)	4.9				

Table 4 : Quasi-static test results on undamaged specimens

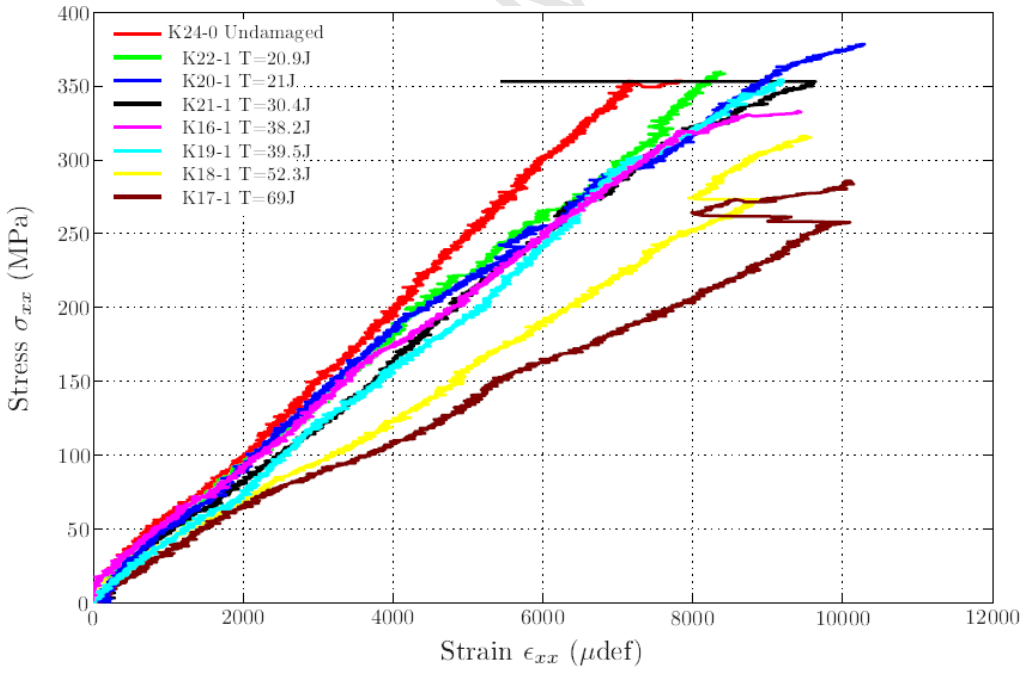

Figure 15 : Stress-strain curves corresponding to quasi-static tests on pre-impacted specimens

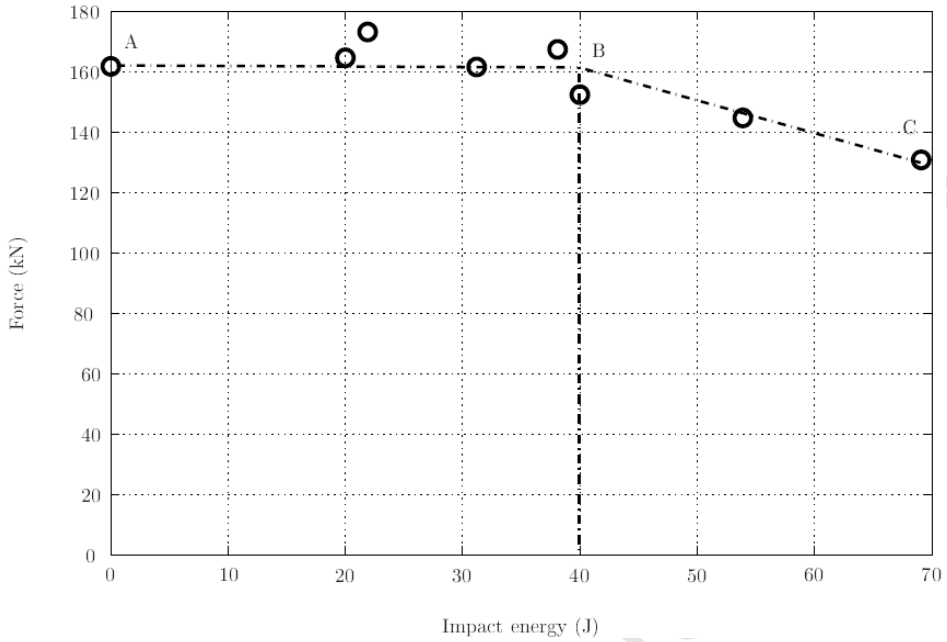

Figure 16 : Force vs impact energy curves corresponding to quasi-static tests on pre-impacted specimens

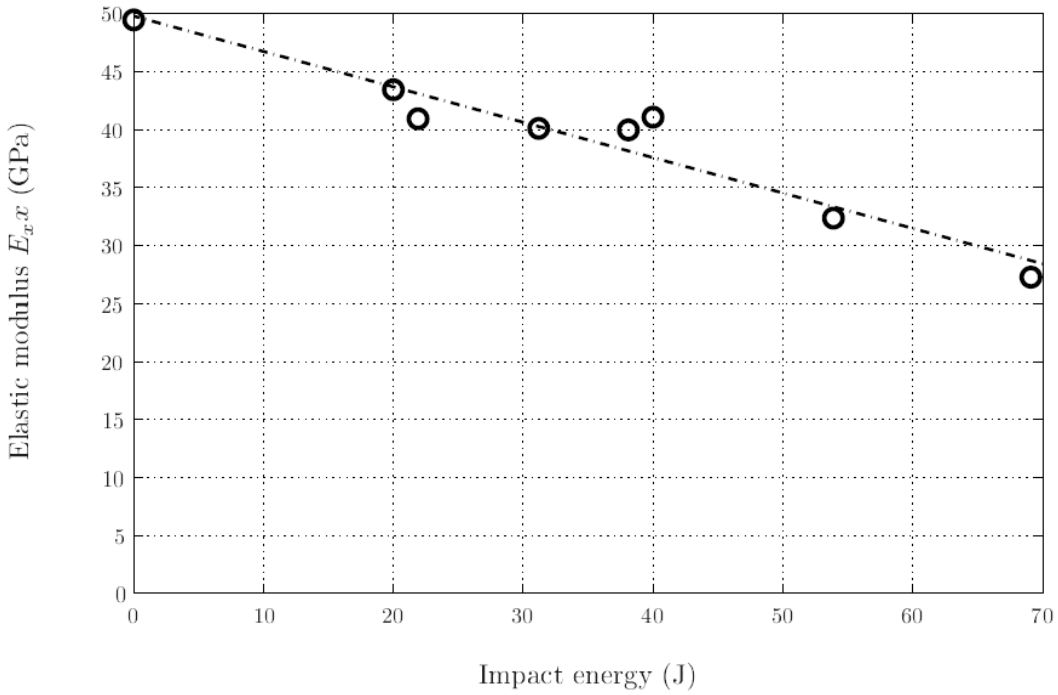

Figure 17 : Homogenized elastic modulus vs impact energy for quasi-static tests on pre-impacted specimens

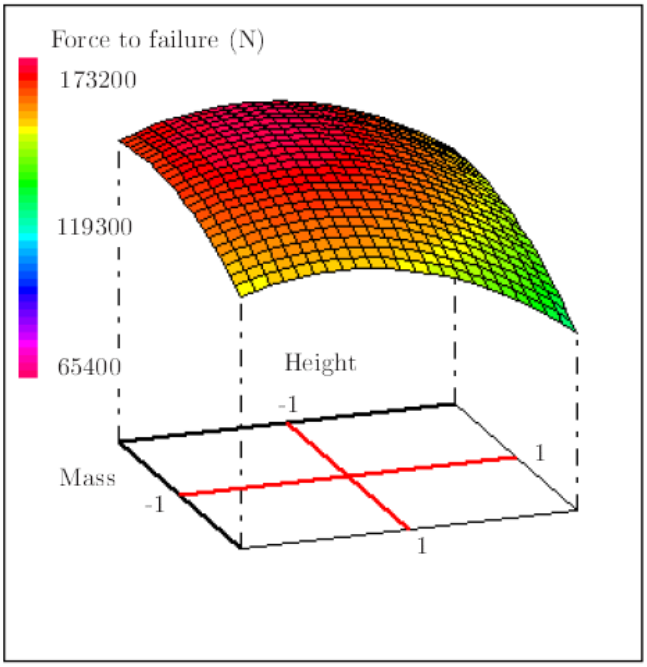

Figure 18 : Isovalues of the response surface corresponding to quasi-static tests on pre-impacted specimens

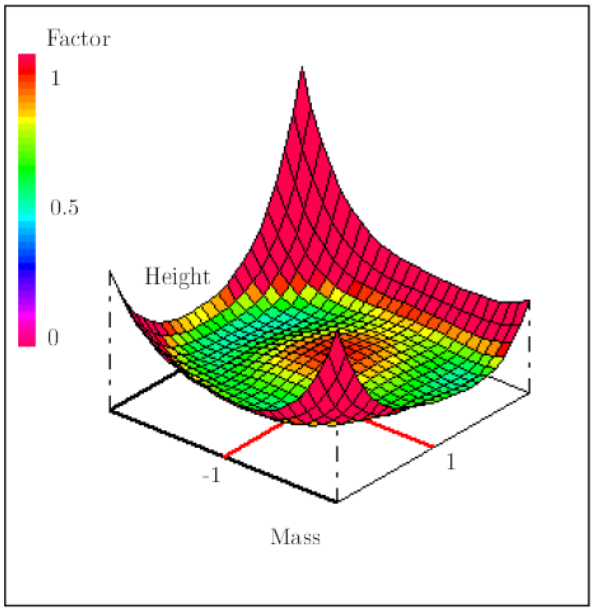

Figure 19 : Variance function

Response	b_0	b_1	b_2	b_{11}	b_{22}	b_{12}
Force to failure	166746	−10745	−10775	−7785	−15342	−2406

Table 5 : Polynomial factors

Source of variation	Summon squares	Degrees of freedom	Average square	Ratio	Signif.
Regression	1.24×10^9	5	2.48×10^8	3.88	36.4
Residues	6.39×10^7	1	6.39×10^7		
Total	1.30×10^9	6			

Table 6 : Variance analysis

Mass (kg)	Height (m)	Experimental force to failure (N)	Model prediction (N)	Deviation (%)
14.48	0.369	144800	148743	2.6
5.96	0.360	173200	170419	1.6
14.48	0.486	130800	128864	1.5
8.09	0.264	164600	168433	2.3
12.35	0.251	161600	158360	2
8.09	0.481	152400	154904	1.6
10.22	0.394	167400	165078	1.4

Table 7 : Model accuracy at the experimental points

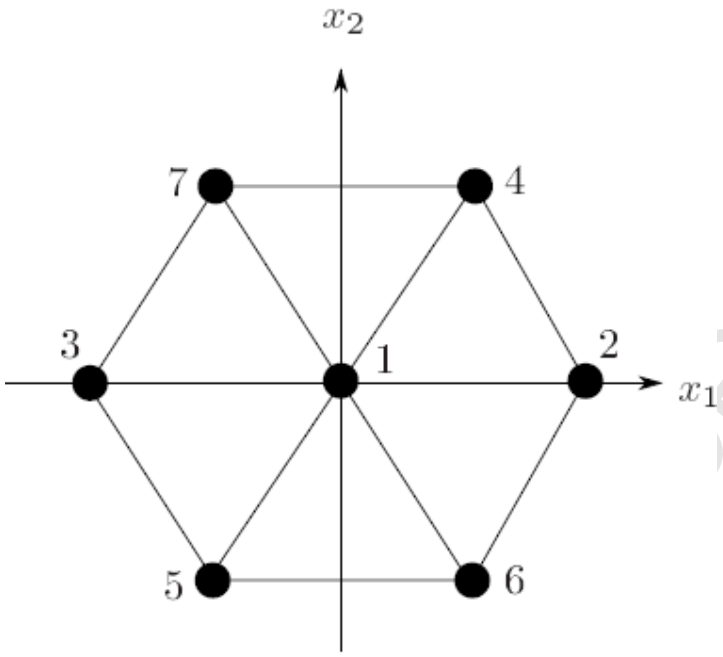

Figure 20 : Doelhert's experimental network in an experimental field with two variables x_1 and x_2

n^o	1	2	3	4	5	6	7
x_1	0	1	-1	0,5	-0,5	0,5	-0,5
x_2	0	0	0	0,866	-0,866	-0,866	0,866

Table 8 : Doelhert's experiments with two variables in centered reduced coordinates